Thallium(I) Acetylacetonate as Building Blocks of Luminescent Supramolecular Architectures[||]

Eduardo J. Fernández,[†] Antonio Laguna,*[,‡] José M. López-de-Luzuriaga,[†] Miguel Monge,[†] Manuel Montiel,[†] M. Elena Olmos,[†] and Javier Pérez[†]

Departamento de Química, Universidad de la Rioja, Grupo de Síntesis Química de La Rioja, UA-CSIC, Complejo Científico Tecnológico, 26001 Logroño, Spain, and Departamento de Química Inorgánica, Instituto de Ciencia de Materiales de Aragón, Universidad de Zaragoza-CSIC, 50009 Zaragoza, Spain

Received September 11, 2003

The heteropolynuclear complexes $[AuTlR_2]_n$ ($R = C_6F_5$, C_6Cl_5) react with [Tl(acac)] in 1:1 or 1:2 molar ratio, leading to products of stoichiometry $[AuTl_2(acac)(C_6Cl_5)_2]$ (**2**) and $[AuTl_3(acac)_2(C_6F_5)_2]$ (**3**). The new complexes obtained display $Tl_2(acac)_2$ units acting as bridges between linear chains of $[AuTl(C_6Cl_5)_2]_n$ in **2** or between $[AuTl(C_6F_5)_2]$ units in **3**. In both structures, in addition to the Au···Tl interactions, Tl(I)···Tl(I) contacts also appear, which are considered to be in part responsible for the luminescent behavior. The comparison of these properties in solution to that of the starting complex [Tl(acac)] allows us to propose the presence of Tl(I)···Tl(I) interactions also in solution. TD-DFT calculations show that $Tl_2(acac)_2$ units would be responsible for the luminescent behavior of Tl(acac) and complexes **2** and **3** in acetonitrile solution.

Introduction

A standard method in the synthesis of supramolecular architectures is the linkage of polyatomic anions with metal centers that can lead to an enormous variety of finite and extended structures. Such phenomena are not limited to the case of anions and also include electron-rich molecules that undergo multiple coordination to the binding sites of Lewis acids.[1] Sometimes, when judiciously chosen, these building blocks can lead to assemblies whose dimensionality can be designed or controlled, which could further permit the design of complexes with appropriate metals and ligands chosen for individual applications.

In this context, the pentahalophenyl gold precursors $NBu_4[AuR_2]$ ($R = C_6F_5$, C_6Cl_5) have been shown as useful starting materials for the rational preparation of a wide variety of heteropolynuclear complexes following the acid−base reaction strategy.[2−9] These, classified as noncluster species, range from discrete molecules[7] to bigger supramolecular assemblies, as extended chains[2−5,8] or two- or three[6]-dimensional networks built only by means of what is generally considered "weak" metal−metal interactions. Nevertheless, a recent theoretical study carried out by our group for the Au···Tl interaction in these systems revealed a surprising strength of 275.7 kJ mol^{-1}, from which 80% is due to an ionic contribution, while the rest is due to dispersion (van der Waals).[8] Taking into account that the interactions appear between closed-shell atoms in +1 oxidation state, it seems plausible that a first key factor that governs the formation of different assemblies is the nature of the perhalophenyl groups. Indeed, as we recently reported, a change of the aryl ligands bonded to gold produces a change in the donor properties of the molecule and, consequently, different metal−metal interactions that give rise to different structures and photophysical properties.[6] The second factor in determining the structural characteristics of the complexes is the nature of the ligands bonded to thallium(I). The position of this center in the periodic table gives it an undefined hard−soft character and, thus, a potential affinity for diverse donor centers, which confers the complex $[AuTl(C_6Cl_5)_2]$ a surprising vapochromic behavior.[9] In addition, thallium(I) displays an astonishing complexity in both its coordination number and geom-

[||] Dedicated to Professor Jose Vicente on the occasion of his 60th birthday.

* To whom the correspondence should be addressed. E-mail: alaguna@posta.unizar.es.
[†] Universidad de la Rioja.
[‡] Universidad de Zaragoza-CSIC.

(1) (a) Hawthorne, M. F.; Zheng, Z. *Acc. Chem. Res.* **1997**, *30*, 267. (b) Hawthorne, M. F. *Pure Appl. Chem.* **1994**, *66*, 245. (c) Wuest, J. D. *Acc. Chem. Res.* **1999**, *32*, 81. (d) Vaugeois, J.; Simard, M.; Wuest, J. D. *Coord. Chem. Rev.* **1995**, *95*, 55.

(2) (a) Usón, R.; Laguna, A.; Laguna, M.; Jones, P. G.; Sheldrick, G. M. *J. Chem. Soc., Chem. Commun.* **1981**, 1097. (b) Usón, R.; Laguna, A.; Laguna, M.; Manzano, B. R.; Jones, P. G.; Sheldrick, G. M. *J. Chem. Soc., Dalton Trans.* **1984**, 285.

(3) Crespo, O.; Fernández, E. J.; Jones, P. G.; Laguna, A.; López-de-Luzuriaga, J. M.; Mendía, A.; Monge, M.; Olmos, E. *Chem. Commun.* **1998**, 2233.

(4) Fernández, E. J.; Gimeno, M. C.; Laguna, A.; López-de-Luzuriaga, J. M.; Monge, M.; Pyykkö, P.; Sundholm, D. *J. Am. Chem. Soc.* **2000**, *122*, 7287.

(5) Fernández, E. J.; Laguna, A.; López-de-Luzuriaga, J. M.; Monge, M.; Pyykkö, P.; Runeberg, N. *Eur. Inorg. Chem.* **2002**, 750.

(6) Fernández, E. J.; Jones, P. G.; Laguna, A.; López-de-Luzuriaga, J. M.; Monge, M.; Olmos, M. E.; Pérez, J. *Inorg. Chem.* **2002**, *41*, 1056.

(7) Fernández, E. J.; López-de-Luzuriaga, J. M.; Monge, M.; Olmos, M. E.; Pérez, J.; Laguna, A. *J. Am. Chem. Soc.* **2002**, *124*, 5942.

(8) Fernández, E. J.; Laguna, A.; López-de-Luzuriaga, J. M.; Mendizábal, F.; Monge, M.; Olmos, M. E.; Pérez, J. *Chem. Eur. J.* **2003**, *9*, 456, and references therein.

(9) Fernández, E. J.; López-de-Luzuriaga, J. M.; Monge, M.; Olmos, M. E.; Pérez, J.; Laguna, A.; Mohamed, A. A.; Fackler, J. P., Jr. *J. Am. Chem. Soc.* **2003**, *125*, 2022.

10.1021/om034167n CCC: $27.50
Publication on Web 01/20/2004

etry,[10] factors that have also been shown to be responsible for the optical properties of these systems.[8]

At this point, we wondered whether the proved affinity of $[AuTlR_2]_n$ with ligands in solution or in solid state can be exploited for the synthesis of higher nuclearity complexes by reacting them with metal complexes containig polydentate donor ligands. Among these, β-diketonato Tl(I) complexes have been revealed as useful precursors in the synthesis of columnar organizations that have even led to the synthesis of metal-organic liquid crystals.[11] In this sense, the amazing coordinative versatility of thallium, the potential formation of Tl(I)···Tl(I) interactions, and the different electronic characteristics of the perhalophenyl groups can play a fundamental role in the organization of the structures.

Then, along with these comments and going on our current interest in the chemistry of heteropolynuclear gold−thallium systems, in this paper we report the study of the reactivity of the complexes $[AuTlR_2]_n$ ($R = C_6F_5$, C_6Cl_5) with [Tl(acac)] (acac = acetylacetonate) and the influence of the factors mentioned above in their structures and, hence, in their optical properties. Finally, we have performed time-dependent DFT (TD-DFT) calculations on $Tl_2(acac)_2$ model systems, which reveal the excitations that lead to emission of light in acetonitrile solution of Tl(acac) and complexes **2** and **3**.

Results and Discussion

Synthesis and Characterization. By reacting equimolecular amounts of $NBu_4[Au(C_6Cl_5)_2]$ and $TlPF_6$ in tetrahydrofuran, the precursor complex $[AuTl(C_6Cl_5)_2]$ (**1a**) is obtained according to the literature procedure.[9] Similarly, $[AuTl(C_6F_5)_2]$ (**1b**) is obtained as a pale yellow solid (see Experimental Section). Both complexes react with [Tl(acac)] (1:1 or 1:2) in toluene, leading to $[AuTl_2(acac)(C_6Cl_5)_2]$ (**2**) or $[AuTl_3(acac)_2(C_6F_5)_2]$ (**3**), showing no dependence on the molar ratio and recovering the excess of [Tl(acac)] or $[AuTl(C_6F_5)_2]$ when the molar ratio is not adequate. Both complexes are moderately soluble in coordinant solvents such as acetone or acetonitrile and insoluble in diethyl ether and hexane. In the solid state they are stable to air and moisture for days or weeks. Their elemental analysis and other physical and spectroscopic properties are in accordance with the proposed stoichiometries. Thus, their IR spectra in Nujol mulls show, among others, absorptions arising from the C_6Cl_5[12] and C_6F_5[2b] groups bonded to gold(I) at 840 and 618 cm^{-1} for **2** and at 1502, 954, and 792 cm^{-1} for **3**, respectively. In addition, the bands due to the acetylacetonate groups appear at 1534 and 1510 cm^{-1} for **2** and at 1560 and 1502 cm^{-1} for **3**, values that are in accordance with the coordination of these groups through their oxygen atoms. Interestingly, their molar conductivities in acetonitrile solutions indicate an ionic formulation with values of 143 (**2**) and 130 (**3**) Ω^{-1} cm^2 mol^{-1}, values typical of 1:1 electrolytes. Nevertheless, the molar conductivity of the precursor complex [Tl(acac)] in the same solvent gives a value of only 3 Ω^{-1} cm^2 mol^{-1}, typical of neutral species, a result that is likely to indicate a covalent bonding in solution between the thallium atoms and the acetylacetonate ligand. Thus, also in accordance with their structures (see below), the dissociative equilibrium that is likely to take place in acetonitrile solution involves the original components of the linear chains, the $[AuR_2]^-$ and Tl^+ ions, while the Tl(acac) units remain associated.

This dissociative equilibrium proposed in solution is confirmed by the solution-state ^{19}F and ^1H NMR spectroscopy, and thus, for complex **3** in D_8-tetrahydrofuran, the signals assigned to the pentafluorphenyl rings appear at values similar to those observed for the precursor complex $NBu_4[Au(C_6F_5)_2]$. By contrast, in the ^1H NMR spectra of **2** and **3** in D_8-tetrahydrofuran, the signals due to the nonequivalent protons of the acetylacetonate groups appear at chemical shifts similar to those of [Tl(acac)], i.e., 5.0 [s, 1H, CH] and 1.72 [s, 6H, CH_3] ppm. At this point, it is worth noting that, in addition, these shifts appear at different values from those obtained in the same solvent for a typical ionic acetylacetonate derivative such as $[N(PPh_3)_2]$(acac), whose resonances appear at 4.7 and 1.56 ppm, respectively.

In short, these results are clearly indicative that [Tl(acac)] behaves as a covalent species in solution and that this fact probably determines the structural motifs obtained in their reactions with ligands or metal complexes.

Crystal Structures. With regard to this, we have determined the crystal structures of complexes **2** and **3** from crystals obtained by slow diffusion of hexane in a saturated solution of the complex in toluene. To compare them with that corresponding to the starting material [Tl(acac)], its crystal structure was also determined by X-ray diffraction. It consists of mononuclear Tl(acac) units in which the acetylacetonate ligands act as chelate and bind the thallium atom through both oxygen atoms with typical Tl−O distances of 2.523(14) and 2.528(9) Å. In the solid, units related by a glide plane are connected via unsupported Tl···Tl interactions of 3.8553(5) Å, a distance longer than the usual relatively short Tl···Tl contacts observed in polynuclear thallium(I) compounds[13] and close to double the van der Waals radium of thallium (1.96 Å).[14] These intermetallic interactions give rise to zigzag unidimensional chains with Tl−Tl−Tl angles of 88.568(15)° that are further interconnected through a bridging oxygen atom of each acetylacetonate ligand (see Figure 1) with a Tl−O distance of 2.826(5) Å, clearly longer than those observed in the Tl(acac) unit. Finally, the Tl−Tl distance between O-bridged Tl(I) centers is 3.9782(5) Å, i.e., longer than the unsupported Tl···Tl interactions and too long to be considered as a intermetallic contact. In short, the structure of [Tl(acac)] in the solid state can be described as an infinite two-dimensional polymer formed via Tl···Tl interactions and oxygen bridges that are probably broken in solution without further dissociation into ions, resulting in molecular Tl(acac) units that are responsible for its molar conductivity.

(10) Wiesbrock, F.; Schmidbaur, H. *J. Am. Chem. Soc.* **2003**, *125*, 3622, and references therein.
(11) Atencio, R.; Barberá, J.; Cativiela, C.; Lahoz, F. J.; Serrano, J. L.; Zurbano, M. M. *J. Am. Chem. Soc.* **1994**, *116*, 11558.
(12) Usón, R.; Laguna, A.; Laguna, M.; Manzano, B. R.; Tapia, A. *Inorg. Chim. Acta* **1985**, *101*, 151.
(13) Janiak, C. *Coord. Chem. Rev.* **1997**, *163*, 107.
(14) Sheldrick, G. M. *SHELXL-97*, A program for crystal structure refinement; University of Göttingen: Göttingen, Germany, 1997.

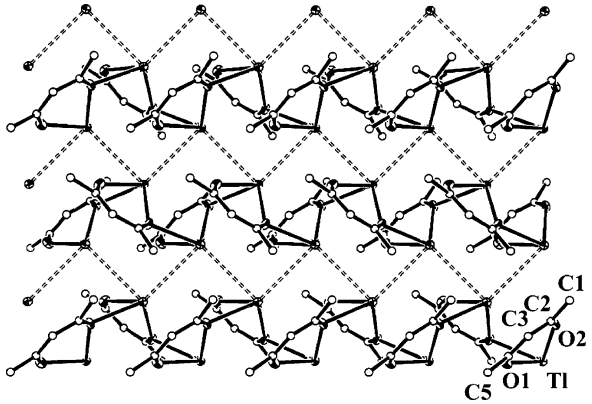

Figure 1. Molecular structure of [Tl(acac)] with the labeling scheme of the atom positions. H atoms are omitted for clarity.

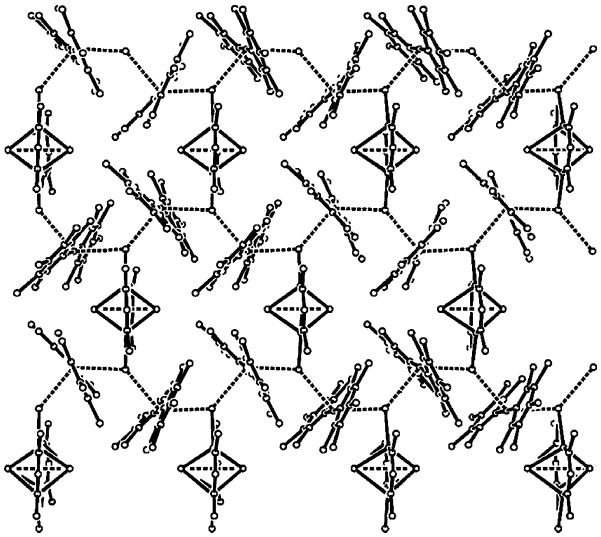

Figure 2. Molecular structure of complex **2**. H atoms are omitted for clarity.

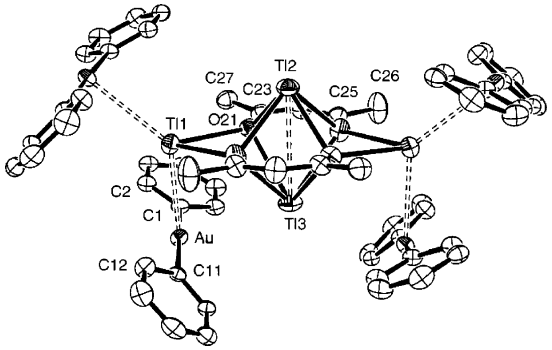

Figure 3. ORTEP diagram for complex **2** (30% probability level) with the labeling scheme of the atom positions. H and Cl atoms are omitted for clarity.

In the case of complex **2**, its crystal structure can be seen as infinite chains formed via unsupported Au···Tl interactions of 3.0963(7) and 3.2468(7) Å (with Tl−Au−Tl and Au−Tl−Au angles of 126.60(2)° and 131.34(2)°) that are joined through $Tl_2(acac)_2$ units acting as bridges between the thallium centers of these chains, giving rise to a two-dimensional structure (see Figures 2 and 3). The gold(I) atoms display their typical linear environment by coordination to two pentachlorophenyl rings with Au−C distances of 2.042(19) and 2.053(10) Å, while Tl(1) binds two bridging oxygen atoms of the $Tl_2(acac)_2$ unit with Tl−O distances of 2.685(8) and 2.676(9) Å, shorter than that of 2.826(5) Å found in the crystal structure of [Tl(acac)]. In the bridging $Tl_2(acac)_2$ unit each thallium(I) center links the four oxygen atoms of the acetylacetonate groups (see Figure 3), showing Tl−O distances within the range 2.653(9)−2.821(8) Å, longer than those described in the mononuclear unit of [Tl(acac)]. Furthermore, the Tl−Tl distance within this dinuclear unit is 3.6774(11) Å, shorter than the unsupported Tl···Tl interactions of 3.8553(5) Å observed in the crystal structure of [Tl(acac)] and similar to some of those described for $MeSi[SiMe_2N(Tl)Bu^t]_3$[15] (3.673(2) Å) or $[H_3CC\{CH_2N(Tl)SiMe_3\}_3][H_3CC\{CH_2NSiMe_3\}_3(H)(Tl)(Li)(thf)]\cdot(toluene)$[16] (between 3.3150(6) and 3.6759(7) Å). Finally, the presence of Au···Cl and Tl···Cl interactions between 3.300(3) and 3.632(3) Å probably contributes to the stability of the system.

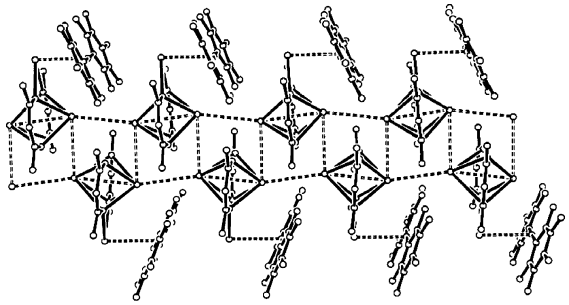

Figure 4. Molecular structure of complex **3**. H atoms are omitted for clarity.

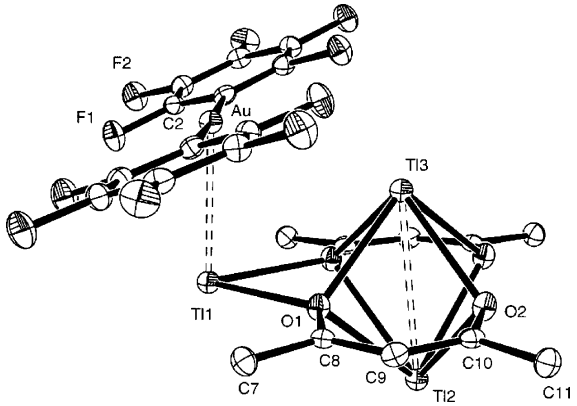

Figure 5. ORTEP diagram for complex **3** (30% probability level) with the labeling scheme of the atom positions. H atoms are omitted for clarity.

On the other hand, the crystal structure of **3** (see Figures 4 and 5) also contains $Tl_2(acac)_2$ and $[AuTl(C_6F_5)_2]$ units linked via two Tl−O bonds of 2.577(3) Å, i.e., closer to the Tl−O distances found in the mononuclear unit of the crystal structure of [Tl(acac)] (2.523(14) and 2.528(9) Å) than to those corresponding to the bridging oxygen atoms of both structures of [Tl(acac)] (2.826(5) Å) and **2** (2.685(8) and 2.676(9) Å). The main difference between the structures of **2** and **3** is that while in the case of **2** the polymerization occurs through Au···Tl interactions and each $Tl_2(acac)_2$ unit bridges two $[AuTl(C_6Cl_5)_2]$ fragments, in **3** it is a consequence of the presence of unsupported Tl···Tl contacts of 3.7200(4) and

(15) Hellmann, K. W.; Gade, L. H.; Scowen, I. J.; McPartlin, M. *Chem. Commun.* **1996**, 2514.
(16) Hellmann, K. W.; Gade, L. H.; Fleischer, R.; Kottke, T. *Chem. Eur. J.* **1997**, *3*, 1801.

Table 1. Details of Data Collection and Structure Refinement for [Tl(acac)] and Complexes 2 and 3

	[Tl(acac)]	complex **2**	complex **3**
chem formula	$C_5H_7O_2Tl$	$C_{34}H_{14}Au_2Cl_{20}O_4Tl_4$	$C_{22}H_{14}AuF_{10}O_4Tl_3$
cryst habit	colorless plate	green prism	colorless prism
cryst size/mm	0.2 × 0.2 × 0.08	0.12 × 0.1 × 0.09	0.2 × 0.12 × 0.08
cryst syst	orthorhombic	orthorhombic	orthorhombic
space group	*Iba*2	*Pbcn*	*Pmna*
a/Å	11.3256(4)	19.4326(3)	7.3260(1)
b/Å	20.6199(5)	10.2815(2)	24.2772(2)
c/Å	5.3836(2)	30.2571(4)	15.2064(3)
V/Å^3	1257.25(7)	6045.26(17)	2704.60(7)
Z	8	4	4
D_c/g cm^{-3}	3.207	2.645	3.297
M	303.48	2406.86	1342.41
F(000)	1072	4288	2360
T/°C	−50	20	−100
$2\theta_{max}$/deg	56	56	56
μ(Mo Kα)/mm^{-1}	25.597	16.376	23.324
no. of reflns measd	9736	7449	44212
no. of unique reflns	833	4834	3295
R_{int}	0.084	0.054	0.055
R [$F>2\sigma(F)$][a]	0.0388	0.0447	0.0242
wR [F^2, all reflns][b]	0.1037	0.1175	0.0532
no. of reflns used	833	48 341	3295
no. of params	76	292	189
no. of restraints	1	77	60
S[c]	1.176	1.061	1.067
max. residual electron density/e Å^{-3}	2.915	1.495	1.720

[a] $R(F) = \sum||F_o| - |F_c||/\sum|F_o|$. [b] $wR(F^2) = [\sum\{w(F_o^2 - F_c^2)^2\}/\sum\{w(F_o^2)^2\}]^{0.5}$; $w^{-1} = \sigma^2(F_o^2) + (aP)^2 + bP$, where $P = [F_o^2 + 2F_c^2]/3$ and *a* and *b* are constants adjusted by the program. [c] $S = [\sum\{w(F_o^2 - F_c^2)^2\}/(n - p)]^{0.5}$, where *n* is the number of data and *p* the number of parameters.

Table 2. Selected Bond Lengths [Å] and Angles [deg] for [Tl(acac)][a]

Tl−O(1)	2.513(14)	Tl−O(2)	2.528(9)
Tl−O(2)#1	2.826(10)	Tl−Tl#2	3.8553(5)
Tl−Tl#3	3.8553(5)	Tl−Tl#1	3.9782(5)
O(1)−C(4)	1.28(2)	O(2)−C(2)	1.27(1)
C(1)−C(2)	1.49(2)	C(2)−C(3)	1.45(2)
C(3)−C(4)	1.41(2)	C(4)−C(5)	1.54(2)
O(1)−Tl−O(2)	71.5(3)	O(1)−Tl−O(2)#1	68.2(4)
O(2)−Tl−O(2)#1	96.9(3)	O(1)−Tl−Tl#2	58.4(2)
O(2)−Tl−Tl#2	129.6(2)	O(2)#1−Tl−Tl#2	70.5(2)
O(1)−Tl-Tl#3	123.3(3)	O(2)−Tl−Tl#3	116.8(2)
O(2)#1−Tl−Tl#3	146.15(19)	Tl#2−Tl−Tl#3	88.568(15)
O(1)−Tl−Tl#1	53.4(2)	O(2)−Tl−Tl#1	58.2(2)
O(2)#1−Tl−Tl#1	39.20(19)	Tl#2−Tl−Tl#1	92.863(3)
Tl#3−Tl−Tl#1	174.162(13)	C(4)−O(1)−Tl	130.6(11)
C(2)−O(2)−Tl	132.5(9)	O(2)−C(2)−C(3)	123.8(14)
O(2)−C(2)−C(1)	117.9(15)	C(3)−C(2)−C(1)	118.3(11)
C(4)−C(3)−C(2)	127.2(11)	O(1)−C(4)−C(3)	126.4(13)
O(1)−C(4)−C(5)	115.7(13)	C(3)−C(4)−C(5)	117.8(13)

[a] Symmetry transformations used to generate equivalent atoms: #1 $-x+1/2, -y+1/2, z-1/2$; #2 $-x, y, z-1/2$; #3 $-x, y, z+1/2$.

3.7607(4) Å and the $Tl_2(acac)_2$ unit links only one [AuTl-$(C_6F_5)_2$] fragment. Thus, complex **3** in the solid state forms a double-chain unidimensional polymer, as shown in Figure 4. The bond lengths and angles within the Tl_2-$(acac)_2$ units are very similar to those found in complex **2** (see Figures 3 and 5 and Tables 3 and 4), showing Tl−O distances in the range 2.658(3)−2.890(3) Å and a Tl···Tl interaction of 3.6688(4) Å (shorter than the unsupported Tl···Tl contacts). Regarding the [AuTl-$(C_6F_5)_2$] fragment, the gold(I) atom displays a linear environment with typical Au−C distances of 2.047(5) Å and a Au···Tl contact of 3.0653(4) Å. Finally, each metallic center shows metal−fluorine contacts within the range 3.208−3.216 Å for gold or 3.218−3.310 Å for thallium that contribute to the stabilization of the structure.

Thus, as we have just commented, the crystal structures of both complexes **2** and **3** contain very similar dinuclear $Tl_2(acac)_2$ and $[AuTl(C_6X_5)_2]$ fragments, but, while in **2** the Au···Tl contacts prevail, in the case of **3** the most important interactions are the Tl···Tl contacts.

Optical Properties. On the other hand, and in addition to their interesting structures, complexes **2** and **3** are luminescent at room temperature and at 77 K in the solid state as well as in solution. Nevertheless, the emissions in the solid state are likely to be greatly influenced by the different structural arrangements that lead to a different number of Au(I)···Tl(I) interactions, as by the presence of $Tl_2(acac)_2$ units attached to the thallium centers.

Complexes **2** and **3** show a single emission at room temperature in the solid state at 531 nm (exc 392 nm) and 429 nm (exc 364 nm), respectively. The different energies of each pair as well as the lifetime measurements seem to indicate a different origin for each complex. In contrast, at 77 K in the solid state, both of them display two independent emissions with two different excitation profiles, appearing at 463 and 588 nm for complex **2** and at 427 and 507 nm for complex **3**. Also, glassy solutions in CH_2Cl_2/EtOH/MeOH at 77 K exhibit intense luminescence, displaying two emissions at 490 and 543 nm for **2** and at 425 and 518 nm for **3** (see Figure 6).

Both complexes are also luminescent in acetonitrile solution, showing a single high-energy emission with virtually identical profile. Thus, complex **2** shows an emission at 390 nm (exc 320 nm), while complex **3** displays an emission at 380 nm by excitation at the same energy. This result is striking from our experience in Au−Tl systems, since, as we have previously reported,[8] the luminescent properties of supramolecular structures built by means of acid−base stacking are lost when dissolved, because the metal−metal interactions

Table 3. Selected Bond Lengths [Å] and Angles [deg] for Complex 2[a]

Au−C(1)	2.042(10)	Au−C(11)	2.053(10)
Tl(1)−O(22)#2	2.676(9)	Tl(1)−O(21)	2.685(8)
Tl(2)−O(21)	2.653(9)	Tl(2)−O(22)	2.693(9)
Tl(3)−O(21)	2.821(8)	Tl(3)−O(22)	2.821(8)
Au−Tl(1)	3.0963(7)	Au−Tl(1)#1	3.2468(7)
Tl(2)−Tl(3)	3.6774(11)		
C(1)−Au−C(11)	177.0(4)	Tl(1)−Au−Tl(1)#1	126.60(2)
O(22)#2−Tl(1)−O(21)	65.9(3)	O(22)#2−Tl(1)−Au	91.1(2)
O(21)−Tl(1)−Au	89.26(19)	O(22)#2−Tl(1)−Au#3	130.5(2)
O(21)−Tl(1)−Au#3	126.96(18)	Au−Tl(1)−Au#3	131.34(2)
O(21)−Tl(2)−O(22)	64.1(3)	O(21)−Tl(2)−O(21)#2	99.5(4)
O(22)−Tl(2)−O(22)#2	98.6(4)	O(21)−Tl(2)−O(22)#2	66.1(3)
O(21)−Tl(3)−O(22)	60.6(3)	O(21)−Tl(3)−O(22)#2	62.4(3)
O(21)−Tl(3)−O(21)#2	91.8(4)	O(22)−Tl(3)−O(22)#2	93.5(4)

[a] Symmetry transformations used to generate equivalent atoms: #1 $-x+3/2$, $y+1/2$, z; #2 $-x+1$, y, $-z+1/2$; #3 $-x+3/2$, $y-1/2$, z.

Table 4. Selected Bond Lengths [Å] and Angles [deg] for Complex 3[a]

Au−C(1)	2.047(5)	Au−Tl(1)	3.0653(4)
Tl(1)−O(1)	2.577(3)	Tl(2)−O(2)	2.729(4)
Tl(2)−O(1)	2.890(3)	Tl(3)−O(1)	2.658(3)
Tl(3)−O(2)	2.689(4)	Tl(2)−Tl(3)	3.6688(4)
Tl(2)−Tl(3)#2	3.7200(4)	Tl(2)−Tl(3)#3	3.7607(4)
C(1)−Au−C(1)#1	177.3(3)	C(1)−Au−Tl(1)	91.14(13)
O(1)#1−Tl(1)−O(1)	65.95(15)	O(1)−Tl(1)−Au	87.02(8)
O(2)#1−Tl(2)−O(2)	64.31(15)	O(2)−Tl(2)−O(1)#1	92.79(11)
O(2)−Tl(2)−O(1)	62.09(10)	O(1)#1−Tl(2)−O(1)	58.08(13)
Tl(3)−Tl(2)−Tl(3)#2	165.068(13)	Tl(3)−Tl(2)−Tl(3)#3	97.911(10)
Tl(3)#2−Tl(2)−Tl(3)#3	97.020(10)	O(1)−Tl(3)−O(1)#1	63.70(15)
O(1)−Tl(3)−O(2)#1	99.13(11)	O(1)−Tl(3)−O(2)	65.70(11)
O(2)#1−Tl(3)−O(2)	65.39(15)	Tl(2)−Tl(3)−Tl(2)#5	82.875(9)
Tl(2)#4−Tl(3)−Tl(2)#5	82.193(9)		

[a] Symmetry transformations used to generate equivalent atoms: #1 x, $-y+1/2$, z; #2 $x+1$, y, z; #3 $x+1/2$, y, $-z+1/2$; #4 $x-1$, y, z; #5 $x-1/2$, y, $-z+1/2$.

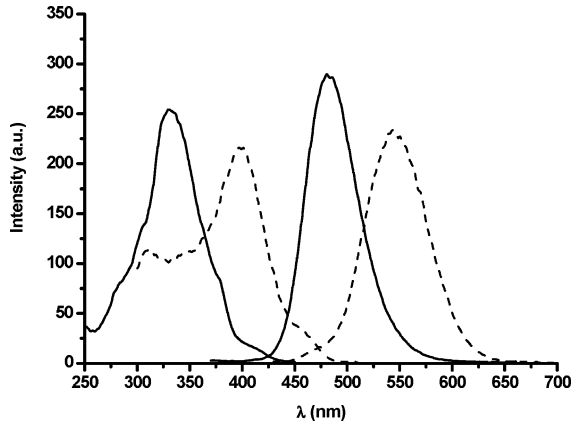

Figure 6. Corrected luminescence spectra of **2** in glass solution (CH_2Cl_2/EtOH/MeOH (1:8:2 v/v)) at 77 K showing two pairs (solid lines and dashed lines) of excitations and emissions.

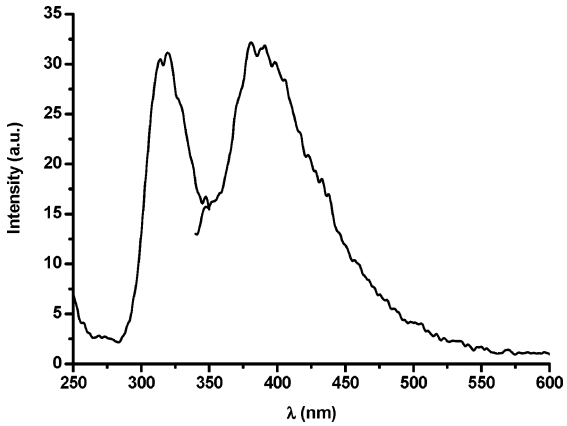

Figure 7. Corrected luminescence spectra of [Tl(acac)] (5×10^{-3} M) in acetonitrile solution.

are no longer present in solution. When the solvent is evaporated, the intermetallic contacts are regenerated and the optical properties are recovered. Thus, the presence of such high-energy emissive states in solution seems to be indicative of a different origin than the gold−thallium interacting centers. In this sense, the perhalophenyl rings in both complexes are not likely to be involved in these transitions, since greater differences in the energy values would be expected if these ligands played an important role. Thus, on the basis of the similar energies found, what it seems likely is that these transitions have their origin in the $Tl_2(acac)_2$ units, which are present in both complexes and, in accordance with our theoretical results, probably, involving orbitals of the thallium and oxygen centers. In fact, the starting complex [Tl(acac)] is luminescent in acetonitrile solution (see Table 5 and Figure 7); nevertheless, its moderate stability in this solvent prevents further lifetime measurements. Thus, excitation at 320 nm gives rise to a blue emission at 390 nm, and [Tl(acac)] as well as complexes **2** and **3** display similar absorptions in their UV−vis spectra with a very intense band located at 314 nm (ϵ = 4400−6600 M^{-1} cm^{-1}), which indicates that this absorption probably gives rise to the emission. UV−vis absorptions assigned to the perhalophenyl ligands are much less intense and have been reported at lower energies.[6] Thus, for complexes **2** and **3** the bands due to the perhalophenyl rings are probably masked by the much more intense absorption at 314 nm. These experimental results and also the DFT

Table 5. Excitation and Emission Spectra and Lifetime Measurements of Complexes [Tl(acac)], 2, and 3

	solution[a] em (exc)	solid (RT) em (exc)	solid (77 K) em (exc)	glass[b] (77 K) em (exc)	τ[c] (ns)
[Tl(acac)]	390 (320)	418 (351)	410 (344)	419 (346)	6453, 230
complex **2**	390 (320)	531 (392)	588 (390)	543 (400)	65, 8
			463 (338)	490 (340)	
complex **3**	380 (320)	429 (364)	507 (386)	518 (380)	7631, 69
			427 (345)	425 (353)	

[a] In acetonitrile (4×10^{-4} M). [b] CH_2Cl_2/EtOH/MeOH (1:8:2). [c] Solid state at room temperature.

calculations carried out on selected models agree with our assignment (see below). Nevertheless, a definite assignment of this band is not possible, since the electronic absorption spectra are fairly featureless.

On the other hand, regarding the solid-state emissions, the starting complex [Tl(acac)] is also luminescent and shows an emission at 418 nm (exc at 351 nm), which is shifted to 410 nm (exc at 344 nm) when the measurement is carried out at 77 K. This blue shift with decreasing temperature is likely to be related to the apparent rigidity (luminescent rigidochromism)[17] that is observed in its two-dimensional structure in the solid state (see above). The comparison of these values with those obtained for complexes **2** and **3** in the solid state at 77 K [462 nm (exc 338 nm) for **2** and 427 nm (exc 345 nm) for **3**] seems to indicate that the higher energy emissions observed in **2** and **3** could have the Tl(acac) units as origin. The shifts found in their energies and with regard to the starting material are likely to be related to the different structural disposition of the Tl(acac) units in [Tl(acac)] and in complexes **2** and **3** (see Figures 1, 3, and 5). Besides, they display a different number of Tl−O and Tl···Tl interactions.

As shown in Table 5, complexes **2** and **3** show a second band at lower energy with independent excitation profiles at 588 nm (exc 390) and 507 (exc 386 nm), respectively. These energies are likely to be attributable to electronic excited states coming from the $d^{10}-s^2$ interactions between gold(I) and thallium(I) centers. In fact, similar energies have been reported previously for thallium−gold systems,[3,6−9,17c,18] and it is worth noting that these emissions do not appear in solution at room temperature, where the Au(I)···Tl(I) interactions are probably lost. Interestingly, the difference in energy observed between both complexes is likely to be due to the different number of Au−Tl interactions present in each complex, since the gold−thallium distances are similar in both structures and such small differences are not likely to be responsible for the shift (ca. 80 nm). Thus, while complex **2** can be considered as extended linear chains of alternating gold and thallium centers bridged by $Tl_2(acac)_2$ units, complex **3** shows only $(C_6F_5)_2Au-Tl$ units bonded to $Tl_2(acac)_2$ moieties (see the structures above). Therefore, as it has been reported in the case of excited states arising from metal−metal interactions, an increase in the number of these interactions leads to a decrease in the energy of the emission bands because the exciton is delocalized along the chain and, consequently, the HOMO−LUMO gap is reduced.[19] In contrast, the break of the polymeric linear structure leads to localized excitons that give rise to emissions of higher energy. An alternative assignment, derived from the difference in basicity of the $[AuR_2]^-$ units ($R = C_6F_5$, C_6Cl_5), could also lead to such findings and cannot be excluded since, according to our previous calculations,[8] these appear in the origin of the electronic transitions.

In contrast, as commented above, at room temperature complexes **2** and **3** display only one emission in the solid state located at very different energies (see Table 5), which suggest very different excited states. Thus, with reference to our previous comments, the emission placed at 531 nm of complex **2** is likely to be related to excited states formed in the interaction among gold and thallium centers, which is probably shifted to high energy if compared with the corresponding low-temperature measurement (588 nm) as a consequence of thermal expansion. By contrast, the energy of the emission of complex **3** (429 nm) is nearer to the band assigned as arising from the $Tl_2(acac)_2$ units (427 nm) for the same complex at low temperature. These values are indicative of a luminescent rigidochromism with increasing temperature. The luminescence lifetime, determined by the phase modulation technique in solid state at room temperature, is in accordance with these assignments because it fits in each case a double-exponential decay with values of 65 and 8 ± 0.05 ns ($\chi^2 = 0.38$) for **2** and 7631 and 69 ± 0.05 ns ($\chi^2 = 0.42$) for **3**, respectively. The short lifetime of the emission in complex **2** is likely to be fluorescence, behavior similar to those found in the previously reported gold−thallium extended linear chains and in which the emissions were assigned as arising from the gold−thallium interactions. In contrast, the lifetime measurement of complex **3**, within the microsecond time scale, is assigned to phosphorescence and is indicative of a different origin, perhaps in the $Tl_2(acac)_2$ units of the complex. In fact, the lifetime of the starting material [Tl(acac)], in solid state, at room temperature, also fits a double-exponential decay with values of 6453 and 230 ± 0.05 ns ($\chi^2 = 0.60$), values near those obtained for complex **3**, which could be indicative of a similar origin in both cases. The fits of the phase and modulation for the double-exponential decay in [Tl(acac)] and complexes **2** and **3** and the normalized residuals are included as Supporting Information. Nevertheless, the shorter lifetimes in

(17) (a) Lees, A. J. *Chem. Rev.* **1987**, *28*, 4623. (b) Ferrandi, G. J. In *Elements of Inorganic Photochemistry*; John Wiley & Sons: New York, 1988. (c) Wang, S.; Garzón, G.; King, C.; Wang, J. C.; Fackler, J. P., Jr. *Inorg. Chem.* **1989**, *28*, 4623.

(18) (a) Wang, S.; Fackler, J. P., Jr.; King, C.; Wang, J. C. *J. Am. Chem. Soc.* **1988**, *110*, 3308. (b) Catalano, V. J.; Bennett, B. L.; Kar, H. M. *J. Am. Chem. Soc.* **1999**, *121*, 10235. (c) Burini, A.; Bravi, R.; Fackler, J. P., Jr.; Galassi, R.; Grant, T. A.; Omary, M. A.; Pietroni, B. R.; Staples, R. J. *Inorg. Chem.* **2000**, *39*, 3158.

(19) Forward, J. M.; Fackler, J. P., Jr.; Asseffa, Z. In *Optoelectronic Properties of Inorganic Compounds*; Roundhill, D. M., Fackler, J. P., Jr., Eds.; Plenum Press: New York, 1999; p 195.

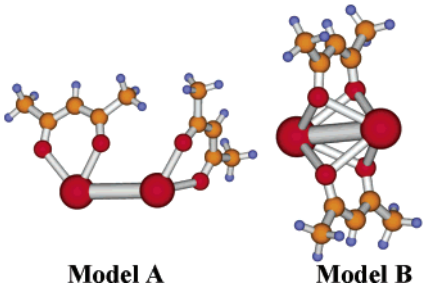

Figure 8. Theoretical model systems: model A is a $Tl_2(acac)_2$ unit built from the X-ray diffraction results from [Tl(acac)]; model B is a $Tl_2(acac)_2$ unit built from the X-ray diffraction results from complex **2** or **3**.

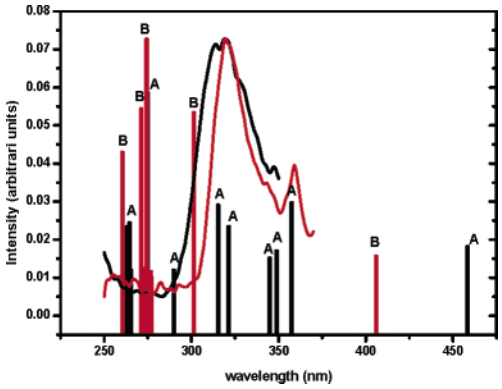

Figure 9. Comparison between theoretical excitation spectra for model systems A and B and experimental excitation spectra for Tl(acac) and complex $[AuTl_2(acac)(C_6Cl_5)_2]$ (**2**).

each case could be also assigned to light scattering instead of fluorescence signals. In short, what is likely to occur at room temperature is that the dominant emissions in complexes **2** and **3** may reasonably be assigned mainly as arising from the gold−thallium interaction and from the $Tl_2(acac)_2$ units, respectively.

Time-Dependent TD-DFT Calculations. The luminescent behavior in solution of [Tl(acac)] and complexes **2** and **3** attributed experimentally to $Tl_2(acac)_2$ units has been studied by time-dependent density functional theory calculations on two different $Tl_2(acac)_2$ model systems built from the X-ray diffraction results (see Figure 8).

The study of the molecular orbitals (MOs) of both model systems A and B shows for the highest occupied orbitals that the most important contribution arises from the $acac^-$ ligands, with an important contribution from the oxygen atoms bonded to the Tl(I) centers (see Supporting Information for population analyses). On the other hand, the shape of the lowest virtual orbitals shows a very important contribution from the Tl(I) centers. Therefore, both models A and B would display transitions arising from ligand-based ($acac^-$) orbitals that arrive to metal-based (Tl(I)) orbitals.

The first few excitation energies up to the ionization limit of models A and B that represent the $Tl_2(acac)_2$ units have been calculated at the TD-DFT level of calculation as described in the computational methods section. We have carried out an analysis of the energy, strength, and orbitals involved for the first singlet excitation energies. On the other hand, as we cannot presently estimate the strength of spin−orbit effects on the triplet transitions, we have analyzed the energy and the orbitals involved in each triplet transition.

Regarding the singlet excitations, the shapes of the predicted excitation spectra for model systems A and B are very similar and also very close (slightly shifted to higher energy values, see Tables 6 and 7) to the experimental excitation profiles of [Tl(acac)] and complexes **2** and **3**, respectively (see Figure 9). In addition, the theoretical maxima for models A and B are displayed at the same energy (274 nm), as observed in the experimental measurements (320 nm, see Table 5). Thus, the analysis of the theoretical excitations confirms

Table 6. TD-DFT RPA Singlet-Excitation Calculations for $Tl_2(acac)_2$ Model A

excitation	λ_{calc} (nm)	λ_{expt} (nm)	oscillator strength[a] (s)	contributions[b]
A	457.9		0.182×10^{-1}	54a ⟶ 57a
B	357.1		0.297×10^{-1}	52a ⟶ 58a (89.0); 56a ⟶ 60a (3.1)
C	348.4		0.170×10^{-1}	56a ⟶ 60a (55.7); 56a ⟶ 59a (13.5); 56a ⟶ 61a (13.4)
D	344.4		0.151×10^{-1}	51a ⟶ 57a
E	321.0	319.5	0.235×10^{-1}	56a ⟶ 61a (39.0); 56a ⟶ 62a (35.6); 51a ⟶ 58a (17.3)
F	314.8		0.291×10^{-1}	53a ⟶ 60a (40.3); 53a ⟶ 59a (29.1); 51a ⟶ 58a (24.1)
G	289.5		0.120×10^{-1}	53a ⟶ 61a (65.6); 56a ⟶ 63a (20.1)
H	274.4		0.586×10^{-1}	54a ⟶ 63a (43.5); 54a ⟶ 59a (21.7)
I	264.7		0.120×10^{-1}	54a ⟶ 63a (37.9); 52a ⟶ 61a (32.0); 53a ⟶ 63a (15.5)
J	264.1		0.245×10^{-1}	51a ⟶ 60a (46.0); 51a ⟶ 60a (30.6); 51a ⟶ 60a (16.6)
K	262.5		0.234×10^{-1}	52a ⟶ 61a (38.3); 53a ⟶ 63a (20.6); 51a ⟶ 59a (20.1)
L	260.2		0.149×10^{-1}	51a ⟶ 59a (47.1); 51a ⟶ 60a (43.0)

[a] Oscillator strength shows the mixed representation of both velocity and length representations. [b] Value is $|coeff|^2 \times 100$.

Table 7. TD-DFT RPA Singlet-Excitation Calculations for $Tl_2(acac)_2$ Model B

excitation	λ_{calc} (nm)	λ_{expt} (nm)	oscillator strength[a] (s)	contributions[b]
A	406.4		0.157×10^{-1}	28a ⟶ 28b
B	301.8	319.5	0.534×10^{-1}	26b ⟶ 30a (44.2); 28a ⟶ 30b (22.6); 27b ⟶ 31a (9.0)
C	280.5		0.245×10^{-1}	28a ⟶ 31a (66.8); 26b ⟶ 31b (24.6)
D	277.7		0.101×10^{-1}	27b ⟶ 31a (51.3); 25b ⟶ 30a (33.0)
E	277.3		0.117×10^{-1}	26b ⟶ 31b (34.8); 28a ⟶ 31a (19.5); 27b ⟶ 31b (13.6)
F	274.8		0.728×10^{-1}	27a ⟶ 29b (27.4); 26b ⟶ 31a (26.9); 28a ⟶ 31b (19.7)
G	273.4		0.125×10^{-1}	25b ⟶ 29b (83.3); 28a ⟶ 31a (8.7)
H	271.7		0.544×10^{-1}	25b ⟶ 30a (44.4); 28a ⟶ 32b (13.9); 27b ⟶ 31a (12.0)
I	260.9		0.430×10^{-1}	27a ⟶ 30b

[a] Oscillator strength shows the mixed representation of both velocity and length representations. [b] Value is $|coeff|^2 \times 100$.

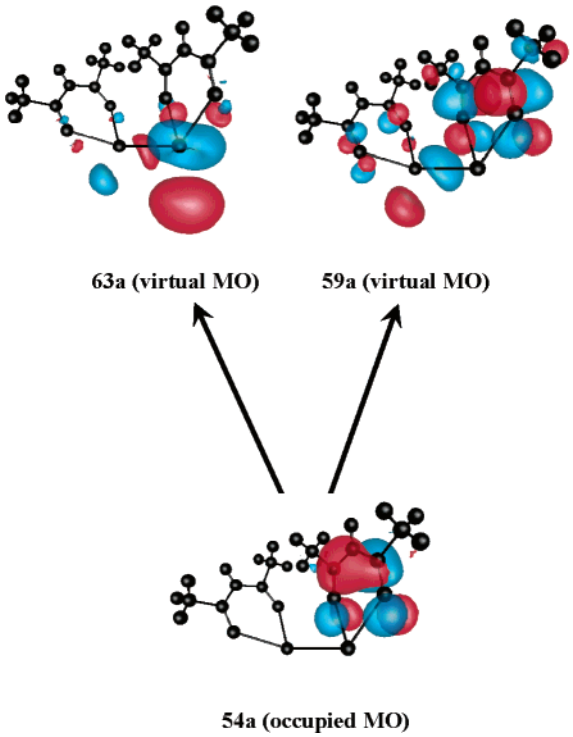

Figure 10. Virtual and occupied MOs involved in the most intense theoretical excitation (274.4 nm) for model A.

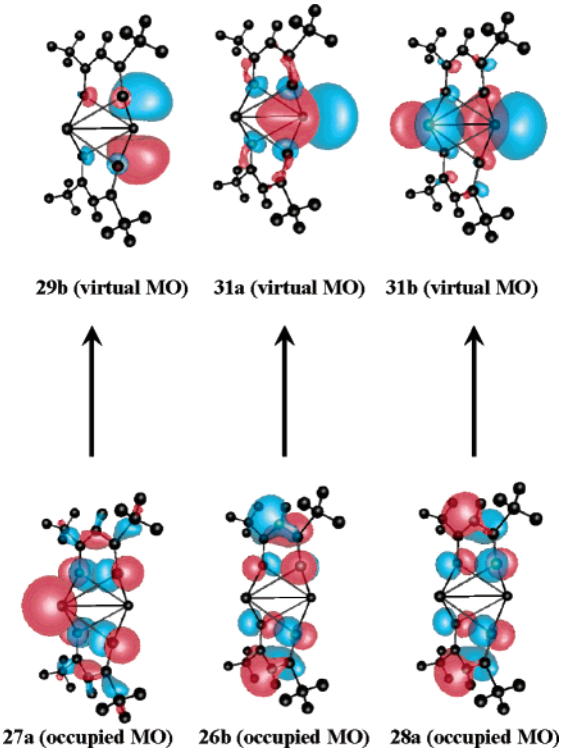

Figure 11. Virtual and occupied MOs involved in the most intense theoretical excitation (274.8 nm) for model B.

that the transitions responsible for the luminescent behavior arise from ligand-based ($acac^-$) orbitals, while the target orbitals are Tl(I)-based molecular orbitals, leading to ligand-to-metal charge transfer character, whereby the Tl(I) centers act as fluorophores in solution (see Figures 10 and 11), in agreement with the experimental results.

Moreover, the most important triplet excitations (in a relative scale, compared to other calculated triplet excitations) are placed at similar and lower energy values (from 274 to 501 nm for model A and from 257 to 450 nm for model B) compared to the singlet excitations of model systems A and B, and their character is also predominantly ligand-to-metal charge transfer character (LMCT) starting from orbitals based on the $acac^-$ ligands and arriving to Tl(I)-based orbitals (see Supporting Information).

Indeed, the fact that both singlet and triplet theoretical excitations show the same LMCT character at similar energy values permits us to suggest that the $Tl_2(acac)_2$ units would be involved in short (nanosecond scale) and long (microsecond scale) lifetimes as observed experimentally for [Tl(acac)] and complex **3**.

Experimental Section

Instrumentation. Infrared spectra were recorded in the range 4000−200 cm^{-1} on a Perkin-Elmer FT-IR Spectrum 1000 spectrophotometer using Nujol mulls between polyethylene sheets. C, H, S analysis were carried out with a Perkin-Elmer 240C microanalyzer. Mass spectra were recorded on a HP59987 A electrospray. ^1H and ^{19}F NMR spectra were recorded on a Bruker ARX 300 in D_8-THF solutions. Chemical shifts are quoted relative to $SiMe_4$ (^1H, external) and $CFCl_3$ (^{19}F, external). UV−visible absorption spectra were obtained on a Shimadzu UV-2401 PC UV−visible recording spectrophotometer in acetonitrile solutions (1×10^{-5} M). Corrected excitation and emission spectra were recorded on a Perkin-Elmer LS-50B luminescence spectrometer. Fluorescence lifetime was recorded with a Jobin-Yvon Horiba Fluorolog 3-22 Tau-3 spectrofluorimeter operating in the phase-modulation mode. The phase shift and modulation were recorded over the frequency range 0.2−50 MHz, and the data fitted using the Jobin-Yvon software package.

General Comments. Thallium(I) acetylacetonate is comercially available and was purchased from Aldrich. The precursor complexes $NBu_4[Au(C_6F_5)_2]$[2b] and $[AuTl(C_6Cl_5)_2]$[12] (**1a**) were obtained according to the literature procedure.

Preparation of $[AuTl(C_6F_5)_2]_n$ (1b). This complex was obtained similarly to **1a**.[9] It is a pale yellow solid. Yield: 83%. Anal. Calcd for **1b** ($C_{12}AuF_{10}Tl$): C, 19.6. Found: C, 20.4. IR: $\nu(C_6F_5)$ 1510, 945, and 788 cm^{-1}. ^{19}F NMR ($CDCl_3$, room temperature, ppm): δ −114.9 (m, 2F, F_o); δ −163.3 (t, 1F, F_p, $^3J(F_p-F_m) = 18.8$ Hz); δ −164.4 (m, 2F, F_m). ES(+) *m/z* (%): 204 $[Tl]^+$ (100). ES(−) *m/z* (%): 531 $[Au(C_6F_5)_2]^-$ (100).

Preparation of $[AuTl_2(acac)(C_6Cl_5)_2]$ (2) and $[AuTl_3(acac)_2(C_6F_5)_2]$ (3). To a solution of [Tl(acac)] (0.06 g, 0.20 mmol) in THF (30 mL) was added $[AuTl(C_6Cl_5)_2]_n$ **1a** (0.18 g, 0.20 mmol) for **2** and $[AuTl(C_6F_5)_2]_n$ **1b** (0.07 g, 0.10 mmol) for **3**. The solution was stirred for 30 min, and the solvent was evaporated in vacuo. The addition of CH_2Cl_2 gave a yellow precipitate for **2** and white for **3**. The solids were filtered off and washed with CH_2Cl_2 (3 × 5 mL). Yield: 74% for **2** and 52% for **3**. Anal. Calcd for **2** ($C_{17}H_7AuCl_{10}O_2Tl_2$): C, 17.0; H, 0.58. Found: C, 17.1; H, 0.60; for **3** ($C_{22}H_{14}AuF_{10}O_4Tl_3$): C, 19.7; H, 1.04. Found: C, 19.2; H, 1.16. IR: $\nu(C_6Cl_5)$ 840 and 618 cm^{-1}; ν(C−O) 1534 and 1510 cm^{-1} for **2**, and $\nu(C_6F_5)$ 1510, 955, and 793 cm^{-1}; ν(C−O) 1560 and 1502 cm^{-1} for **3**. ^1H NMR (D_8-THF, room temperature, ppm): δ 5.01 (s, 1H, CH); δ 1.75 (s, 6H, CH_3) for **2**; ^1H NMR (D_8-THF, room temperature, ppm): δ 5.02 (s, 1H, CH); δ 1.77 (s, 6H, CH_3). ^{19}F NMR (D_8-THF, room temperature, ppm): δ −114.9 (m, 2F, F_o); δ −163.3 (t, 1F, F_p, $^3J(F_p-F_m) = 18.8$ Hz); δ −164.4 (m, 2F, F_m) for **3**. ES(+) *m/z* (%): 204 $[Tl]^+$ (100) in both cases, and 304 $[Tl - acacH]^+$ (75) for **3**. ES(−) *m/z* (%): 695 $[Au(C_6Cl_5)_2]^-$ (100) for **2** and 531 $[Au(C_6F_5)_2]^-$ (100) for **3**.

Crystallography. Crystals were mounted in inert oil on glass fibbers and transferred to the cold gas stream of a Nonius

Kappa CCD diffractometer equipped with an Oxford Instruments low-temperature attachment. Data were collected using monochromated Mo Kα radiation ($\lambda = 0.71073$ Å). Scan type: ω and ϕ. Absorption corrections: numerical (based on multiple scans). The structures were solved by direct methods and refined on F^2 using the program SHELXL-97.[14] All non-hydrogen atoms were refined anisotropically. Hydrogen atoms were included using a riding model. Further details of the data collection and refinement are given in Table 1. Selected bond lengths and angles are collected in Tables 2−4 and crystal structures of [Tl(acac)] and complexes **2** and **3** in Figures 1−5. CCDC-210929−210931 contain the supplementary crystallographic data for this paper. These data can be obtained free of charge via www.ccdc.cam.ac.uk/conts/retrieving.html (or from the Cambridge Crystallographic Data Center, 12 Union Road, Cambridge CB2 1EZ, UK; fax: (+44) 1223-336-033; or e-mail: deposit@ccdc.cam.ac.uk).

TD-DFT Calculations. The molecular structures used in the theoretical studies of $Tl_2(acac)_2$ model systems A and B were taken from the X-ray diffraction results for [Tl(acac)] and $[AuTl_2(acac)(C_6Cl_5)_2]$ (**2**) or $[AuTl_3(acac)_2(C_6F_5)_2]$ (**3**) (similar $Tl_2(acac)_2$ units), respectively. Keeping all distances, angles, and dihedral angles frozen, single-point DFT calculations were performed on the models. In both the single-point ground-state calculations and the subsequent calculations of the electronic excitation spectra, the default Beck−Perdew (B−P) functional[20−22] as implemented in TURBOMOLE[23] was used. The excitation energies were obtained at the density functional level using the time-dependent perturbation theory approach (TD-DFT),[24−28] which is a density functional theory generalization of the Hartree−Fock linear response (HF-LR) or random phase approximation (RPA) method.[29]

In all calculations, the Karlsruhe split-valence quality basis sets[30] augmented with polarization functions[31] were used (SVP). The Stuttgart effective core potentials in TURBOMOLE were used for Tl.[32] Calculations were performed without assuming any symmetry for model A and assuming a C_2 symmetry for model B.

Acknowledgment. This work was supported by the D.G.I.(MCYT)/FEDER (BQU2001-2409). M. Montiel thanks C.A.R. for a grant.

Supporting Information Available: Phase and modulation curves and normalized residuals of complexes **1**, **2**, and **3**. Tables S1 and S2 show the population analyses for the highest occupied orbitals for model systems A and B, respectively. In Tables S3 and S4 the most important triplet theoretical excitations are displayed. This material can be obtained, free of charge, via the Internet at http://pubs.acs.org.

OM034167N

(20) Vosko, S. H.; Wilk, L.; Nusair, M. *Can. J. Phys.* **1980**, *58*, 1200.
(21) Perdew, J. P. *Phys. Rev. B* **1986**, *33*, 8822.
(22) Becke, A. D. *Phys. Rev. B* **1988**, *38*, 3098.
(23) Ahlrichs, R.; Bär, M.; Häser, M.; Horn, H.; Kölmel, C. *Chem. Phys. Lett.* **1989**, *162*, 165.
(24) Bauernschmitt, R.; Ahlrichs, R. *Chem. Phys. Lett.* **1996**, *256*, 454.
(25) Bauernschmitt, R.; Ahlrichs, R. *J. Chem. Phys.* **1996**, *104*, 9047.
(26) Bauernschmitt, R.; Häser, M.; Treutler, O.; Ahlrichs, R. *Chem. Phys. Lett.* **1997**, *264*, 573, and references therein.
(27) Gross, E. K. U.; Kohn, W. *Adv. Quantum Chem.* **1990**, *21*, 255.
(28) Casida, M. E. In *Recent Advances in Density Functional Methods*; Chong, D. P., Ed.; World Scientific: Singapore, 1995; Vol. 1.
(29) Olsen, J.; Jørgensen, P. In *Modern Electronic Structure Theory*; Yarkony, D. R., Ed.; World Scientific: Singapore, 1995; Vol. 2.
(30) Schäfer, A.; Horn, H.; Ahlrichs, R. *J. Chem. Phys.* **1992**, *97*, 2571.
(31) Dunning, T. H., Jr. *J. Chem. Phys.* **1994**, *100*, 5829.
(32) Andrae, D.; Haeussermann, U.; Dolg, M.; Stoll, H.; Preuss, H.; *Theor. Chim. Acta* **1990**, *77*, 123.